The Use of the Monte-Carlo Method to Simulate High-Energy Radiography of Dense Objects

Michael J. George
Karl H. Mueller
Rosemary H. O'Connor
Robert G. Schrandt

DISCLAIMER

DISTRIBUTION OF THIS DOCUMENT IS UNLIMITED

MASTER

THE USE OF THE MONTE-CARLO METHOD TO SIMULATE

HIGH-ENERGY RADIOGRAPHY OF DENSE OBJECTS

by

Michael J. George, Karl H. Mueller,
Rosemary H. O'Connor, and Robert G. Schrandt

ABSTRACT

Recently a series of experiments were done at the National Institutes of Health where radiographic scatter was measured at beam energies from 8 to 22 MeV. We have used the Monte-Carlo method to calculate the scattered radiation intensity in the configuration of these experiments. The existing Los Alamos MCNP (Monte-Carlo Neutron Photon) code was modified to include electron transport, and the variance-reduction schemes available in that code were extensively applied to the problem. Beam collimation has been modeled and studied, as has a narrow-hole collimator behind the film plane for the elimination of scatter. The calculations show that the scattered radiation intensity, with respect to the direct radiation, is minimized at beam energies in the range of 15–20 MeV. When a gap in the experimental collimator is included in the model, the absolute value of the direct-to-scattered radiation ratio is in agreement with the experimental data. The simple idea of a small radiographic source size allowing the scattered radiation to be reduced relative to the direct by moving the object closer to the source is also borne out by these calculations. Preliminary results are presented on off-axis scattered radiation. This work provides a foundation for future modeling and design of radiographic experiments.

I.   INTRODUCTION

In 1981 the Hydrodynamics Group proposed the construction of a dual-axis radiographic facility based on pulsed diode machines producing 30–100 R at 1 m with a peak energy of 4–6 MeV. The intended application was standard weapons development radiography yielding more information by virtue of dual views with independent timing.

By 1986, the applications had evolved to include, as a major task, the radiography of features in dense objects. This is a difficult objective

requiring optimization of as many of the radiographic parameters as possible. From the standpoint of the x-ray source, the electron energy, dose, and source spot size are critical parameters. Based only on the fraction of the original x-ray beam that is transmitted through areal masses of interest, the optimum electron source energy is -10-12 MeV. This ignores the very real problem of scattered radiation. With transmissions on the order of $10^{-4} - 10^{-5}$ scattered radiation can constitute a major part of the flux incident on a detector.

With these issues in mind, a series of experiments were carried out at the National Institutes of Health (NIH) covering an energy range from 8-22 MeV (1). These experiments indicated that there was a peak in the ratio of direct (transmitted) radiation to scattered radiation for electron source energies between 15 and 20 MeV. The experiments were predicated on the use of narrow angle collimation at the detector plane to "reject" scattered radiation and thus separate the direct and scattered components.

The true nature of the performance of this collimation was not known and constituted the major uncertainty in the experimental results. Monte Carlo transport codes are capable of treating this type of problem and providing the detailed picture of scattered and direct radiation contributions at the detector. Further, the codes can indicate the major sources of scatter, leading to understanding how to improve radiographic experiment design. We needed this detailed information to validate the experimental results.

The most trusted electron-photon transport code is Cyltran or one of its derivatives (members of the ITS series) (2). For problems involving modest attenuations and favorable geometries these codes provide acceptable results in less than an hour of Cray CPU time. Unfortunately, our problem meets neither of these criteria and we were faced with the prospects of 10-100 hour run times to obtain marginal results.

The Los Alamos code MCNP (3) is a mature code treating coupled neutron-photon transports and is equipped with numerous tools and special features to treat extreme attenuation and complex geometries encountered in shielding calculations. The decision was made to use a special version of MCNP which

would incorporate the physics of the ITS codes into the framework of the geometry specification and biasing of the MCNP code. The NIH experimental arrangement was modeled and successfully run using the modified code MCNP-E.

II.   USE OF THE MCNP-E CODE

MCNP (3) is a neutron-photon transport code of the Los Alamos Radiation Transport group, X-6. MCNP-E is a modification to MCNP, where the electron data and physics are taken from the ITS (2) codes. The geometry, source routines, tally structure, and variance reduction features are all those of MCNP. Geometrical features include surface specifications, volume cell definitions, and coordinate transformations. Source routines allow for the specification of the input particle source at run time or for the reading of a surface source generated by a previous problem. A variety of output tally types are available, supplemented by diagnostic information regarding the origin and characteristics of particles contributing to the tallies. The variance reduction features are designed to produce lower statistical error estimates in the tallies by doing multiple calculations on those particles that make the most significant contributions. For example, "splitting" can be done on photons, with corresponding weight reductions, based on the importance of the originating cell, direction of propagation, or energy above a specified threshold. Thus, a single large contribution to a tally can be converted to numerous small contributions.

One of these variance reduction schemes is a point detector (4) option, which allows one to better calculate the flux or intensity at a specified point or region of space. From a particle source or at collision points, the fraction of the beam scattering in the direction of the detector is calculated, together with the attenuation to region of the detector. The calculated particles thus "flow" toward the region of interest, while propagation toward other regions is done with less statistical precision. This method is particularly valuable in regions of space like an image plane, where very few source particles cross this plane.

A variation of the point detector scheme involves defining a sphere, called a DXTRAN (5) sphere, around a tally region or a region of importance. Such a region can be determined from knowledge, either from first principles or from previous code output, that many particles that contribute to a tally must pass through a localized region of the problem geometry. Pseudo-particles are then transported from source or collision points to the surface of this sphere and stored for later transport. The scattering fraction and attenuation factor are modifications to the weight given to the particle. Regular tallies are then made inside this sphere, or else these particles are transported as desired above to a surface source or a second DXTRAN sphere.

We introduce here the "standard" problem geometry, upon which most of the calculations to date are based. The upper part of Fig. 1 is a scale drawing showing the configuration of the four basic physical elements of the problem: (left to right) source, collimator, object, and detector. Key position values, in mm, along the radiographic beam (z) axis are given. This is essentially the configuration of the NIH experiments. The lower part of the figure shows each of the four elements in greater detail. The details of the collimator and detector will be discussed later. The object is a standard spherical test object used at the Hydrodynamics (6) Group. The radii of the void, depleted uranium (D-38), copper, and foam are 10, 45, 65, and 225 mm, respectively. The size and shape of the void at the center represent features for investigation. For the present discussion, the image plane is at the front face of the detector at z=2.96 m; other variations will be discussed later.

In calculations of dense-object radiography in the configuration of Fig. 1, MCNP-E was used to determine the direct and scattered photon radiation at the image plane. The problem source was a monodirectional, monoenergetic electron beam impinging on a tungsten target. The primary source of photons was the first-order bremsstrahlung particles produced in the target.

The direct and scattered radiation were calculated separately. For the direct problem, a DXTRAN sphere of radius 10 mm was centered on the image

plane on the axis of symmetry. A source electron was followed to a point where a bremsstrahlung photon was to be generated. The photon energy was next sampled. Then a point was sampled uniformly in area on the DXTRAN sphere and a pseudo-photon transported along this direction to the sphere. The photon weight was modified by the attenuation factor and a factor based on sampling along this direction from a probability distribution function (7) for bremsstrahlung scattering. If a beam of electrons all produced bremsstrahlung photons at this collision point, these weight reductions would represent the fraction of the beam emitted at this angle that reached the image plane with no further collisions. Subsequently, a direct tally on the image plane was made with this particle. The electron tracking was then resumed.

For the scattered problem, a DXTRAN sphere was positioned near the collimator (radius 120 mm, 2 = 1137.5 mm) on the axis but on the image side of the collimator. This was to ensure a good sampling of photons getting through the collimator. The pseudo-photons were then transported as described above from the source target (tungsten) to the DXTRAN sphere. Subsequently, these photons were retrieved from storage and tracked through the dense object sphere. A second DXTRAN sphere was located at the image plane, similar to the direct problem. Photons scattering in the dense object geometry then produced a second set of pseudo-photons on this sphere. The scattered tally on the image plane was then made from these particles.

In general the total photon energy arriving at the detector was tallied, rather than the total number of particles, because we believed this would be a better simulation of the response of radiographic film. The important contribution to the direct and scattered radiation was those high-energy bremsstrahlung photons emitted in a small angle from the axis of symmetry. The energy distribution was biased to sample more high-energy photons (8). This method was particularly effective in getting relatively high-energy scattered photons over to the image plane. The biasing of the photon's initial direction was effected by the radius and position of the DXTRAN sphere.

Some of the other biasing schemes of MCNP were employed in a somewhat conservative manner to augment the DXTRAN approach. These included cell importance sampling, additional particle splitting on energy, and directional splitting for collisions in the dense object geometry.

The scattered problem was run in two parts. In the first part, the pseudo-particles transported to the first DXTRAN sphere were then written as a surface source on the front (left) outer hemispherical surface of the object. The second part started with this source and tracked the particles through the dense object geometry. At each particle collision, the fraction of the beam reaching a selected point on the image plane was calculated, similar to the direct radiation contribution. The particle tracking was then resumed. Subsequently, a tally was made representing this scattered contribution to the image plane. Splitting the problem allowed experimenting with different cell configurations and importance sampling in the dense object sphere without having to repeat the first part. Furthermore, when later problems were to be run with changes in either the object or the detector, they could be started with the same surface source.

The biasing schemes of MCNP are supported with extensive diagnostic outputs, which help one understand some of the large tallies. For example, the weight distribution of pseudo-photons on the DXTRAN sphere is broken down by the cell of the collision or source point. For many of the scatter problems, the object was divided into 170 cells, so that we could better understand the origin of the scattered radiation. A lot of the large scattered tallies appear to come from high-energy photons that are not transmitted through the dense central part of the object but rather scatter in the foam around the heavy metal and back toward the axis. We could then take advantage of cell-importance splitting to improve the statistical errors associated with the large tallies.

Despite the speed of the CRAY XMP computer, these calculations would not be feasible without the use of variance reduction schemes like the bremsstrahlung energy biasing and the DXTRAN approach.

III. RESULTS OF PROBLEMS

Our immediate goal is to understand the scattered radiation field, which involves multiple events that depend on position, direction, and energy. Except for source broadening effects, the calculation of the direct radiation is fairly straightforward, essentially amounting to line integrals along monodirectional paths. However, the separate calculation of the direct radiation helps us affirm the credibility of the code, and it gives insight toward our understanding of the scattered radiation.

A.   Direct-to-Scattered Radiation Ratio

This is similar to a signal-to-noise ratio, in the sense that all the useful radiographic information is contained in the direct radiation, while the scattered component produces a non-image-forming background exposure. For this study we ran problems at five source energies: 6, 10, 17, 25, and 30 MeV. The first of these energies corresponds approximately to the lowest energy in the NIH experiments (representing pulsed diode technology), while the last corresponds to the PHERMEX machine running under optimum tuning. An important question to be investigated is whether there is an optimum energy where the direct-to-scattered ratio can be maximized.

The first problems were run with the object at 1.5 m from the source. Later the object was moved to 2.0 m, and it remained there for all further studies. The results at all five energies for the two positions are shown in Fig. 2, where the direct-to-scattered intensity ratio is plotted as a function of energy. Indeed the curves both seem to show a broad maximum in the vicinity of 17 MeV, or slightly higher. The differences between the two curves can be nearly explained by making the approximation that the scattered radiation behaves like an inverse square source centered about 100 mm downstream from the object center. Because of the collimator, the total illumination of the object by the direct radiation is the same at both positions. The advantage to be gained by moving the object closer to the source is obvious, although other considerations, such as spot-size blurring,

may mitigate against this approach. When constructing new radiographic machines, however, the advantage of minimizing the spot size becomes obvious.

B. Film Response Function

If the results of the MCNP-E calculations are to be compared with experimental radiographs, it is important to make the calculational detector respond to radiation as a function of energy in a way analogous to the experimental detector which is a radiographic film with a heavy-metal conversion screen. The screen converts photons to electrons (photoelectric, Compton, and pair production), and the ionization tracks of the electrons activate the film emulsion. This process tends to be more efficient at the lower photon energies, because most of the electrons are relativistic, and, therefore, the number of ions per unit length of track is nearly independent of energy. The MCNP-E code has the capability of folding a response function of energy into the tallies to mimic the radiographic film response.

A typical film pack consists of a light-metal front plate, heavy-metal front screen, double-emulsion film, heavy-metal back screen, and light-metal back plate. In the NIH experiments, the light-metal plates were 10-mm-thick beryllium, and the heavy-metal screens were 1-mm-thick lead. In a dynamic experiment the plates would be needed for blast protection, and they would probably be aluminum. The screens are most commonly lead, but other materials such as tantalum or platinum could be used, and the thickness could vary. Normally a stack of screens and films is used, the back screen for one film serving as the front screen for the next film, etc.

We have used the ITS codes to calculate the energy deposited in the film for several input photon energies. Ten-mm beryllium plates were used, and calculations were done for 0.1, 0.25, 0.5, and 1.0-mm lead screens. The results are shown in Fig. 3. The two curves for each screen thickness show separately the front and back film emulsions, the curve of more broken texture always being the back emulsion. The 1.0-mm screen shows a response that is nearly proportional to the incident photon energy, while the 0.1-mm screen tends to provide relatively more response from the lower-energy photons. An

-8-

earlier calculation was done with 0.1-mm lead screens and 1.0-mm beryllium plates, yielding the response function shown in Fig. 4, giving an even stronger weighting toward the low energies.

Because we have done many calculations with the function of Fig. 4 folded into the output, we will use the label "energy deposited" for those results below, while the label "energy incident" will be applied to tallies of total energy without any further response function. We will claim that any real result, with response functions like those in Fig. 3, will lie between the incident and deposited results, and we hope to emphasize that any conclusions that we reach are not strongly dependent on any particular film-response function.

We generally expect the scattered radiation to be shifted toward lower energies as compared with the direct radiation. The net effect of a response function, such as that of Fig. 4, should be an emphasis of the scattered radiation and consequently a lowering of the direct-to-scattered ratio. The actual results, for the object at 2.0 m from the source, are given in Fig. 5, now also showing the error estimates for the calculations as computed by the code. The results of the NIH experiments are also shown in this figure. The reconciliation between the experiments and the calculations will be discussed below in connection with the graded and multi-hole collimators.

C.   Energy Spectra

The output tallies are broken into energy bins selected by the user, and therefore the energy spectrum of any tally is immediately available. As a typical example for the reader, Fig. 6 shows the spectra of both the direct and scattered components of the incident photon energy, from a 17-MeV electron source, arriving at a 10-mm-radius detector in the film plane. Figure 7 shows the equivalent spectra for the energy deposited in the film, obtained by folding in the response function of Fig. 4.

Similar results have been obtained for the other four energies for which we have run problems. They all show a broad maximum without any apparent fine structure. Because the film-response function also contains no

sharp structure, we believe that our output calculations will not show any strong energy dependence, and the use of additional intermediate energies for the input source will generally not be necessary. This situation may be different at energies below 0.5 MeV, where the photoelectric absorption edges begin to become important, but for the problems under consideration here, that part of the spectrum makes only a small contribution to the total.

D.   Effect of the Collimator

The purpose of the collimator is twofold. First, it is desirable to suppress the direct beam incident on the outer parts of the object that project off the edge of the film or are otherwise uninteresting, so that these parts of the object do not become sources of scattered radiation that will contaminate the image in the region of interest. Second, especially by the use of the "graded" collimator as shown in Fig. 1, one can produce a graded attenuation as a function of radius that will reduce the dynamic range of intensities to be recorded on a single film. In practice the collimator should also be large enough to suppress scatter from external material, such as the ground.

Figure 1 shows three collimator configurations that have been studied: graded, fine, and coarse. Most problems have been run with the full graded configuration, where the inner radius projects well inside the outer radius of the uranium. In the fine configuration, the entire conical inner surface projects through the foam at approximately mid-radius. The coarse configuration corresponds to essentially no collimation at all, but it may still be useful for suppressing ground scatter. MCNP-E runs have been made at 6 and 25 MeV source energy with all three collimator configurations.

The direct radiation on the axis should be unaffected by the removal of collimator elements, because the inner radius of even the graded collimator projects outside the 10-mm-radius detector. This has been confirmed by the calculations. At 25 MeV, the direct radiation decreased by 1.5% in going from graded to coarse, while at 6 MeV it increased by 4%. These changes are within the statistical error estimates of the calculations. The scattered radiation

is very strongly affected, however. At 25 MeV, with respect to the scattered intensity in the graded configuration, and with the film response function folded in, the scattered intensity went up by a factor of 75 in the fine configuration and a factor of 207 in the coarse configuration. The corresponding results at 6 MeV were factors of 68 and 264, respectively. In terms of energy incident on the film, the respective factors were 99 and 226 at 25 MeV, and 80 and 264 at 6 MeV. An attempt to measure the graded-to-fine increase at 25 MeV experimentally yielded a factor of 30±20.

The above results suggest that the direct-to-scattered radiation ratio is very sensitive to small changes in the details of the collimation. A recent review of the NIH experiments has served to remind us that there was a physical gap at the interface between the graded and fine collimators, which caused a bright ring of direct radiation to appear on the film about 150 mm from the axis. The question then arises as to what effect this additional direct radiation through the object has on the scattered radiation observed on the axis. The size of the gap is not documented. We made a guess of 0.25 mm and set it up in an MCNP-E problem with 25-MeV source energy. Compared with our earlier run without a gap, the scattered radiation on the axis increased by a factor of 1.73 for energy incident and 1.41 for energy deposited. The direct radiation on the axis is, of course, unchanged. Therefore, the calculated results for 25 MeV in Fig. 5 would be reduced by the same factors. We have not calculated the effect of the gap at the other energies, but we believe similar results would be obtained. Thus, the two curves in Fig. 5 are brought into much better agreement with the experimental data.

E.   The Multihole Collimator

The multihole collimator has been used experimentally as a ruse to differentiate between direct and scattered radiation. It is shown in Fig. 1 as a thick block of lead to the right (downstream) of the film plane with a single 6.35-mm-diameter hole concentric with the axis. In reality here are many holes, all drilled with their axes parallel to the divergent direct beam.

The fundamental assumption is that the scattered radiation is sufficiently divergent in angle, so that only a negligible amount of it can propagate all the way through the hole to a second film plane at the back of the lead. Therefore only direct radiation is measured at the back film plane, while direct plus scattered is recorded at the front film plane. The difference between the front reading and the back reading, corrected for the beam divergence, is the scattered intensity. Presumably, this quantity, measured at many locations in the film plane, would allow fitting or modeling of the scattered radiation field, which could then be subtracted from the image recorded on the front film. The NIH experiments were interpreted in this way.

In the analysis of data from the multihole collimator, the largest uncertainty is whether a significant amount of scattered radiation can still reach the back film plane; realize that the wall of the hole itself can be a source of scattered radiation. This problem can be calculated directly with MCNP-E, and so we can shed some light on the interpretation of the NIH experiments. We have calculated the radiation arriving on a 6.35-mm-diameter disk at the back film plane and divided it into four categories: first, direct-direct (DD) radiation, that radiation that was direct upon arrival at the front film plane and reached the back film plane without alteration; second, scattered-direct (SD), direct radiation at the front film plane that gave rise to scattered radiation at the back film plane; third, scattered-scattered (SS), scattered radiation at the front film plane that underwent further scattering before arriving at the back film plane; and fourth, direct-scattered (DS), scattered radiation at the front film plane that arrived at the back film plane without further scattering. Only the DD radiation is desirable. Table I gives the percentages of radiation arriving at the back film plane that fall into each category at the five source energies studied. The results indicate that the DD radiation makes up about 92% of the total, nearly independent of source energy, and not strongly dependent on which response function is used. The error estimates in the SD and SS categories are often as much as 25%, because the detector is very small, and relatively little radiation is reaching it.

TABLE I

RADIATION AT BACK FILM PLANE

Percent in each Category

Energy (MeV)	Energy Incident				Energy Deposited			
	DD	SD	SS	DS	DD	SD	SS	DS
6	92.5	5.5	2.0	0.0	91.5	6.3	2.2	0.0
10	89.7	7.9	2.4	0.0	90.2	7.1	2.7	0.0
17	92.3	3.1	4.6	0.0	91.8	3.8	4.4	0.0
25	94.4	3.7	1.8	0.1	93.7	4.1	2.1	0.1
30	93.3	2.6	4.1	0.0	92.6	3.2	4.1	0.1

For each energy, the simulation of the NIH experiments proceeds as follows. All radiation components at the back film plane are added together, because there was no way to separate them in the real experiments. The sum is then corrected according to the inverse square law to get the "direct" radiation at the front film plane; this correction factor is 1.11. This result is then subtracted from the total (direct + scattered) radiation calculated at the front film plane to get the "scattered" radiation at the front film plane. The direct-to-scattered ratio so obtained is plotted in Fig. 8 at the various source energies. The relatively large statistical error estimates come from the subtraction step mentioned above.

The effect of the graded/fine collimator gap has been calculated indirectly by assuming that the scattered component at the front film plane, and the SS and DS components at the back film plane, increase by the factors given above. At 25 MeV source energy, the "energy incident" point in Fig. 8 moves from 2.54 down to 1.78, and the "energy deposited" point moves from 1.81 down to 1.40. If we assume that similar result would be obtained at the other

energies, then the curves of Fig. 8, with their estimated errors, will overlap the experimental data in Fig. 5.

We wish to emphasize that the results in Fig. 8 are a calculational simulation of the NIH experimental data in Fig. 5. When the gap in the graded collimator is estimated and taken into account, the calculations seem to be in reasonable agreement with the experimental data. The calculations in Fig. 5, however, remain the most direct and accurate representation of the direct-to-scattered ratio as a function of energy. With any film pack that would likely be used experimentally, the true situation should lie between the two calculated curves in Fig. 5.

F.   Total Radiation at Different Energies

Another summary of the results discussed above is shown in Fig. 9, where the direct and scattered components at the front film plane are plotted as a function of energy. These are the "energy incident" calculations. The increased bremsstrahlung production efficiency at the higher energies is emphasized here. While the intensity increases as the 2.5 to 3.0 power of the energy, more or less as expected, we should remember that it has been modified by transmission through the object. The direct-to-scattered radiation ratio is proportional to the vertical distance between the two curves on the log-log plot.

G.   Off-Axis Calculations

All of the results reported above have involved detection of photons on a 10-mm-radius disk centered on and normal to the radiographic axis. For the multihole collimator calculations, a separate tally was generated for the central 3.175-mm radius. Only very recently have we begun expanding the calculations to larger distances from the axis. Our detector, still in the film plane, has been expanded to a radius of 150 mm and divided into concentric rings of width 10 mm. Several problems have been run with the DXTRAN sphere at different radii in order to try to optimize the statistical error in various portions of the disk. A new surface source was recently

generated at the front hemisphere of the object for 3×10^6 17-MeV source electrons and used for this problem. All other calculations reported above used 3×10^5 source electrons. The results for "incident energy" are shown in Fig. 10. Here the flux in each ring has been divided by the average flux over the entire 150-mm-radius disk from one of the problems. This represents the scattered radiation field over an area equivalent to the largest film that we use experimentally. The field appears to be quite flat as a function of radius. If the scattered radiation is truly uniformly distributed in angle from the object, then the inverse square effect would cause about a 2.5% decrease in going from the center to 150-mm radius. However, there is reason to believe that the scattered radiation may increase at larger radii from the axis. At radii beyond 130 mm the graded collimator, which is a source of scattered radiation, comes into view from behind the copper part of the object. At even larger radii, more of the front side of the object can be seen in the manner of a crescent moon, illuminated by direct radiation, with resulting scatter paths of low attenuation. Clearly more work will be needed, possibly at even larger distances from the axis. So far these calculations have been done only at 17-MeV source energy.

H.   General Remarks

Some Monte-Carlo calculations have been done at Lawrence Livermore National Laboratory that appear to be in mild contradiction to the results reported above (9). The scattered radiation is only the order of 10% of the total, compared with more like 25% here. There appears to be more structure as a function of radius in the film plane, and the dependence of the direct-to-scattered ratio seems to be less than what we have calculated, although only two source energies were tried.

The significant difference is that the Livermore calculations were done to model a particular dynamic experiment in great detail, including the massive film-protection system, where our calculations have keyed on the NIH experiments, which used no heavy film protection. A thick layer of material in front of the film will preferentially attenuate scattered radiation, but,

of course, it creates scattered radiation of its own. To a certain extent, the film-protection system will probably act in a way similar to the multi-hole collimator by attenuating scatter in a manner that is less dependent on source energy. Furthermore, because most of the scatter is then produced near the film, more structure as a function of radius off the axis can be expected. Clearly the inclusion of heavy film-protection materials should be one of our goals for future work.

IV. CONCLUSIONS AND FUTURE PLANS

We believe that the MCNP-E code has effectively simulated the NIH experiments, confirming and enhancing our understanding of the results. We now have a better assessment of the multihole collimator and its limitations. Even more important, we now have a tool for calculating directly what has been hard to measure experimentally, the scattered radiation field. If we believe the maximization of the direct-to-scattered radiation ratio is a good criterion for selecting a source energy, then our results point toward a source energy in the 15 to 20 MeV range.

Among our immediate future goals will be a continuation of the study of the scattered radiation off axis. In particular, we plan to study the scatter field at large angles from the axis, probably on a spherical surface rather than in the film plane. The results should merge with those of Fig. 10. This problem will be pertinent to our planned Dual-Axis Radiographic Hydrotest facility (DARHT), where the scattered radiation from one beam will contribute to the exposure of the film on the other beam.

Our ultimate goal is to use MCNP-E as a tool to help us design experiments and understand their results. In most cases, parametric studies can be done more unambiguously and more easily, although not necessarily more precisely, with the code than in real experiments. Problems of interest include collimator design and placement, variations in the object to better simulate dynamic experiments, and the details of radiation transport through a film pack. As mentioned above, the effects of the film-protection system are

expected to be important and should be studied carefully. The code is fully three-dimensional, so we should not be limited to axisymmetric problems.

ACKNOWLEDGMENTS

Joseph M. Mack deserves recognition for the initial proposal that the Monte-Carlo method could be used to calculate radiographic scatter. He provided significant guidance in the formulation of the original problems used in this study. Special mention should be given our colleagues at the French CEA, who contributed to the concept and development of the multihole collimator. The "object" used in these calculations was designed for mutual studies and has come to be known as the "French Test Object".

REFERENCES

1. Karl H. Mueller, "Optimum Energy for Dense Object Flash Radiography," Los Alamos National Laboratory report M-4:GR-87-6 (August 1987).

2. "ITS: The Integrated Tiger Series of Coupled Electron/Photon Monte Carlo Transport Codes," Sandia National Laboratory report SAND84-0573-UC-32 (November 1984).

3. "MCNP — A General Monte-Carlo Code for Neutron and Photon Transport — Version 3A," Los Alamos National Laboratory report LA-7396-M, Rev. 2 Manual UC-32 (September, 1986).

4. Ref. 3, pp 87 and 323.

5. Ref. 3, pp 128 and 246.

6. Karl H. Mueller, "Collimation Techniques for Dense Object Flash Radiography," Proc. 16th International Congress on High Speed Photography and Photonics, Strasbourg, France, August 27-31, 1984 (SPIE, Bellingham, Wash., 1984) Vol. 491, pp 130-136.

7. Robert G. Schrandt, "MCNP-E — Bremsstrahlung Uncollided Photon Contribution to Point Detector or DXTRAN Sphere," Los Alamos National Laboratory memorandum X-6:RGS-88-153 (March 30, 1988).

8. Joseph M. Mack, "Biasing of Bremsstrahlung Energy Distribution" (in preparation).

9. David R. Goosman, Livermore National Laboratory, private communication.
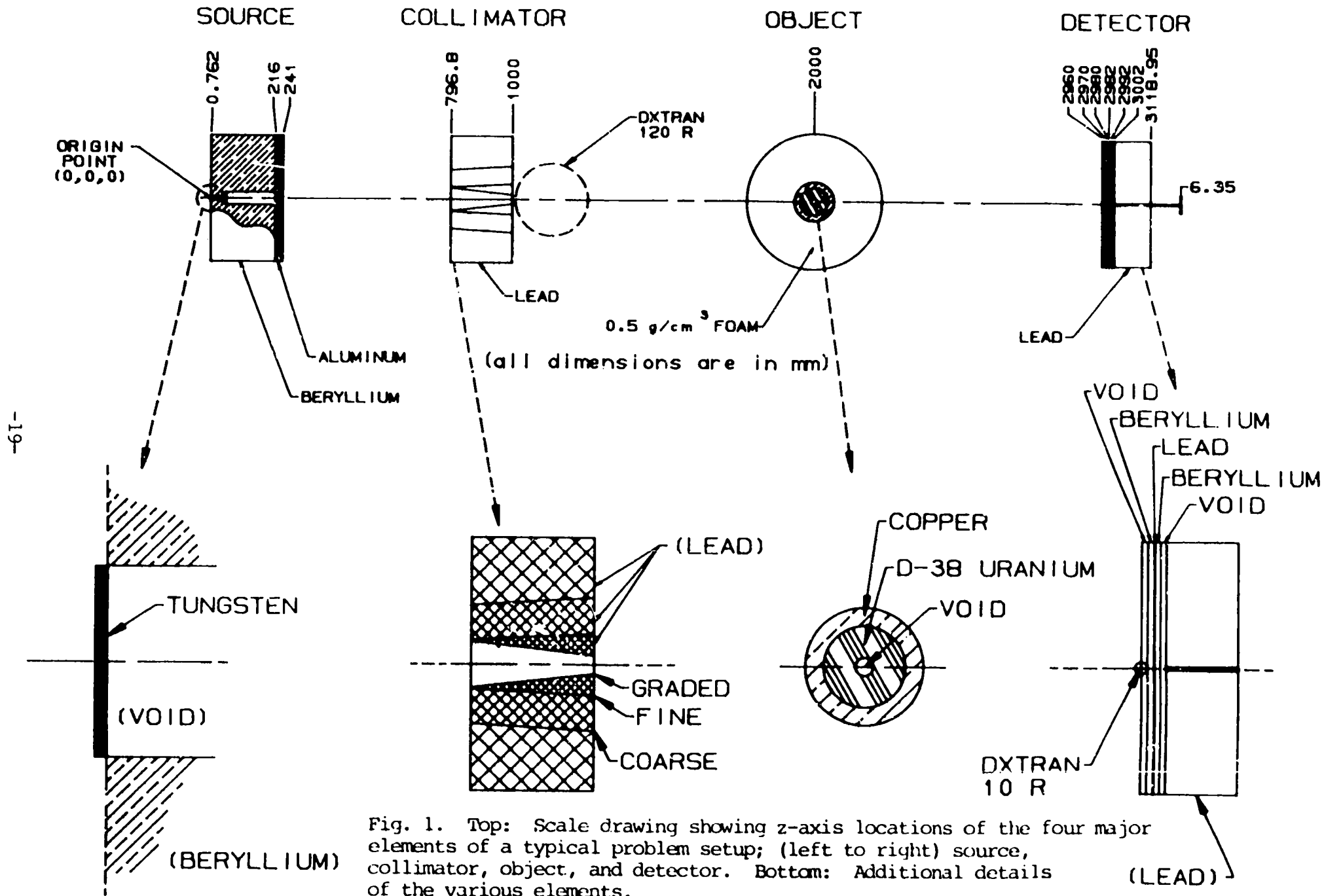
MONTE-CARLO SIMULATION GEOMETRY

Fig. 1. Top: Scale drawing showing z-axis locations of the four major elements of a typical problem setup; (left to right) source, collimator, object, and detector. Bottom: Additional details of the various elements.
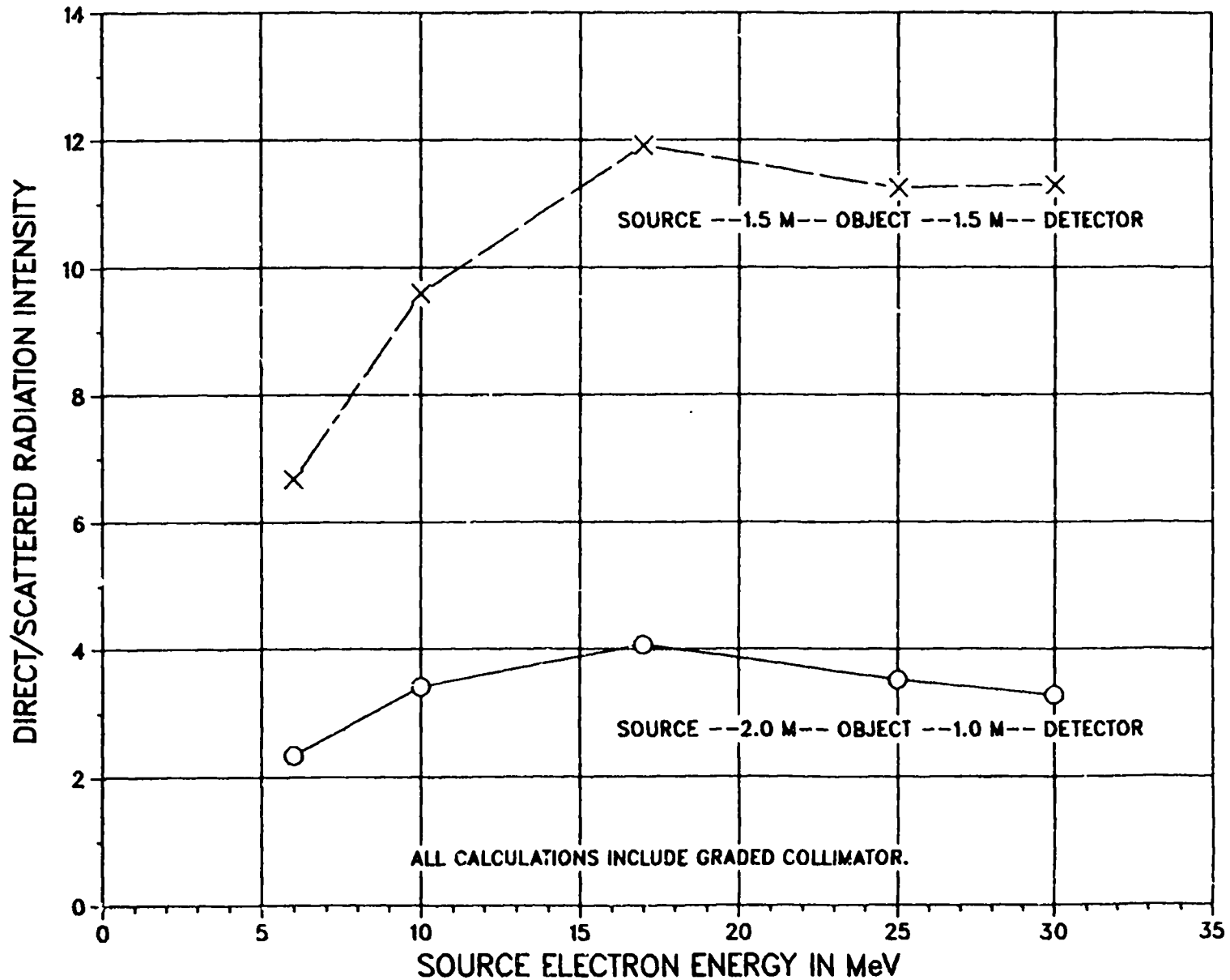
-19-

MCNP—E CALCULATIONS
NIH EXPERIMENT CONFIGURATION

Fig. 2. The direct-to-scattered radiation intensity has been calculated at five source energies for two positions of the object, other elements remaining fixed. Both show a maximum at 17 MeV.

CYLTRAN CALCULATIONS
FILM RESPONSE CURVES

ENERGY DEPOSITED IN FILM EMULSION IN keV PER INCIDENT PHOTON

1.0-MM Pb SCREENS

0.5-MM Pb SCREENS

0.25-MM Pb SCREENS

0.1-MM Pb SCREENS

ALL CALCULATIONS INCLUDE 10.0-MM Be SCREENS

INCIDENT PHOTON ENERGY IN MeV
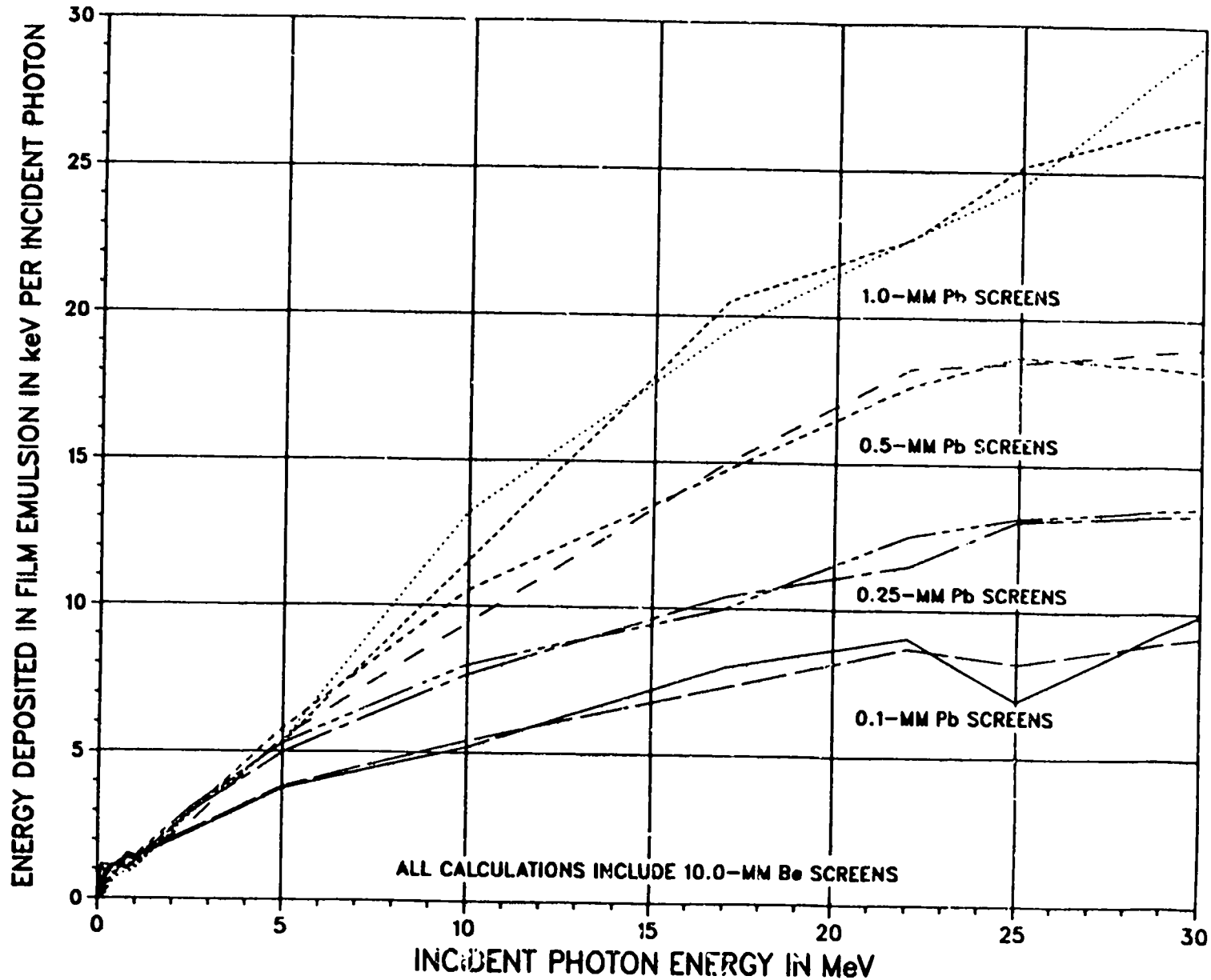
Fig. 3. Energy deposited in film emulsion for various photon energies has been calculated with the ITS Cyltran code for four thicknesses of lead screens on both sides of the film. For each screen thickness, the more solid (broken) curve is for the front (back) film emulsion.

MCNP–E CALCULATIONS
FILM RESPONSE FUNCTION
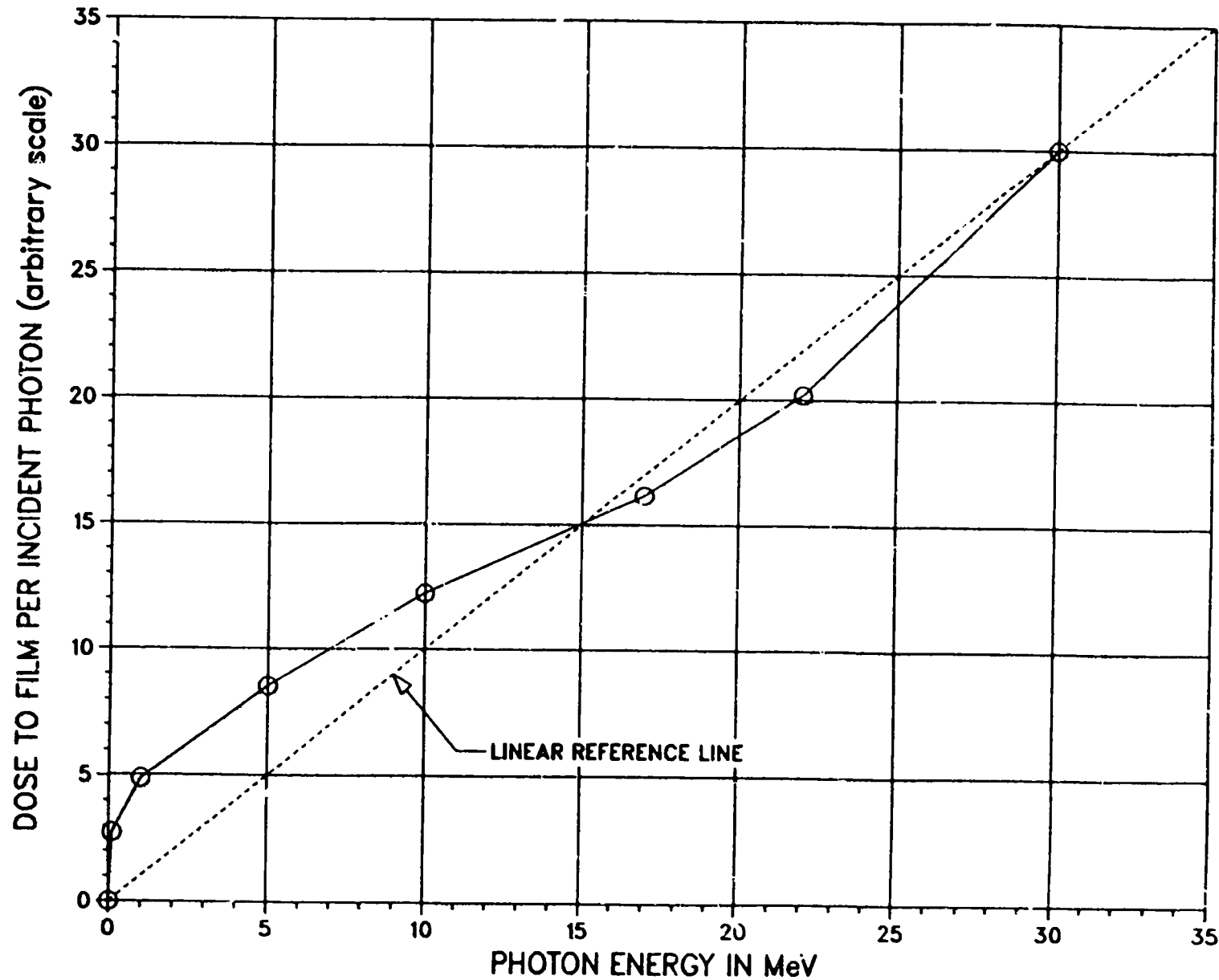
Fig. 4. This "film response" function corresponds to the lower curve of Fig. 3, but with 1.0-mm-thick Be screens. It has been folded into many of our MCNP-E outputs on a photon by photon basis and identified as "Energy Deposited." The linear line is "Energy Incident," or intensity.
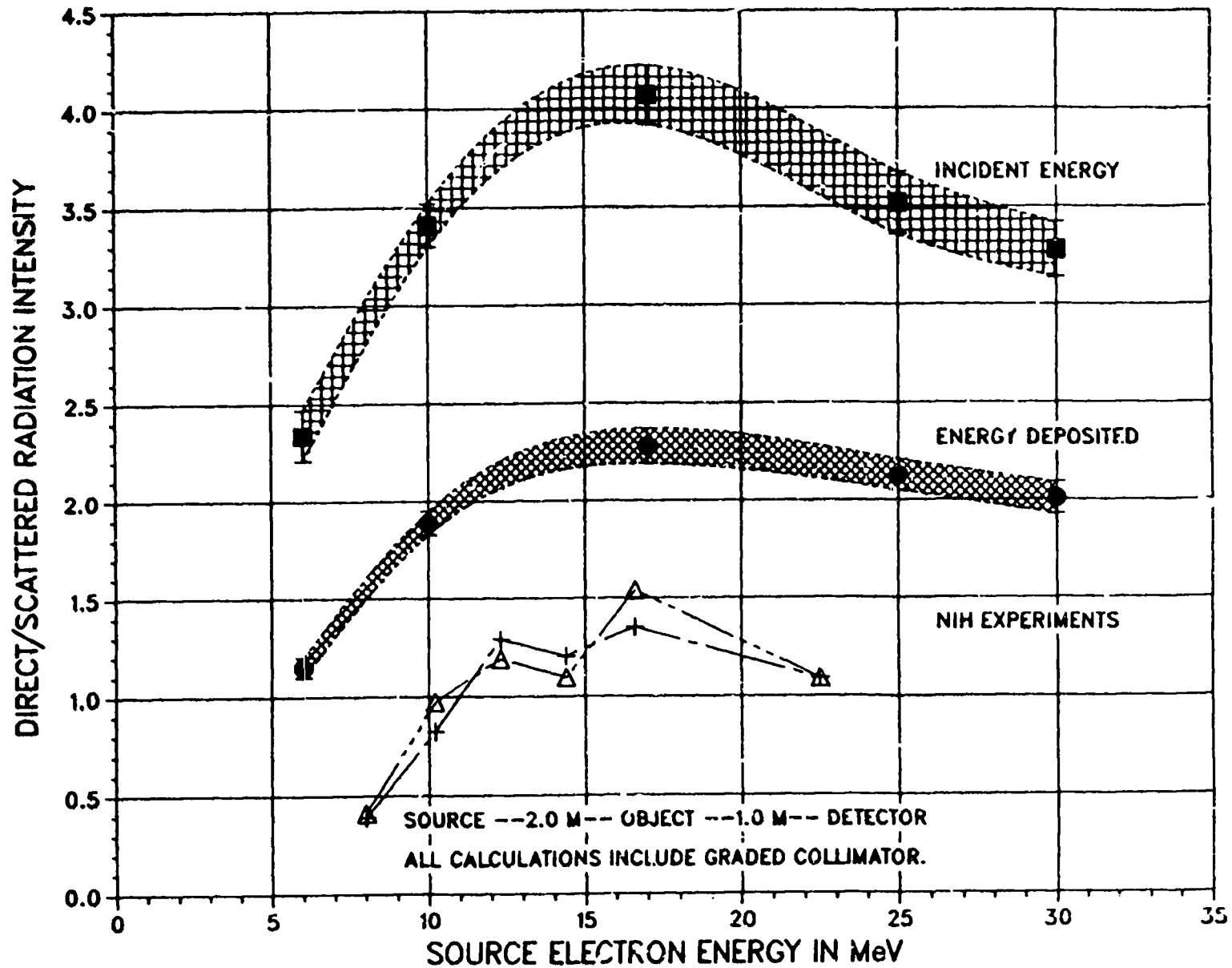
Fig. 5. The lower curve of Fig. 2 is reproduced here, with estimated errors, as the "incident energy" curve. The result of folding in the film-response function of Fig. 4 is the "energy deposited" curve.

17—MeV ENERGY SPECTRUM
Energy Incident on Film Plane

Legend

◩ Direct—I

◩ Scattered—I

Intensity per MeV (Arbitrary Units)

Photon Energy (MeV)
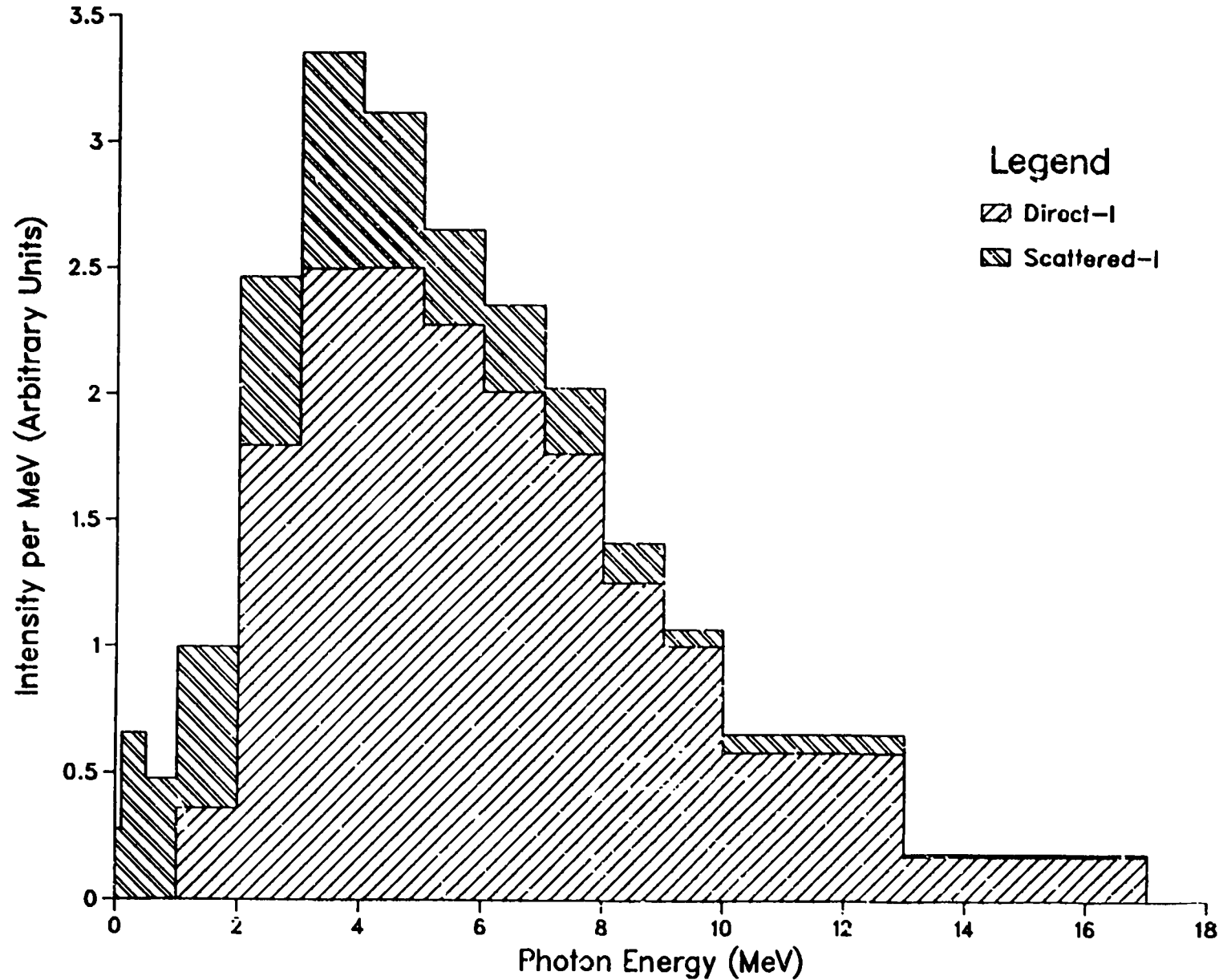
Fig. 6. 17-MeV energy spectrum for radiation incident on the film plane, showing both direct and scattere' components. The scattered component has a lower average energy. Similar results ai : obtained at other energies.

17—MeV ENERGY SPECTRUM
Energy Deposited in Film
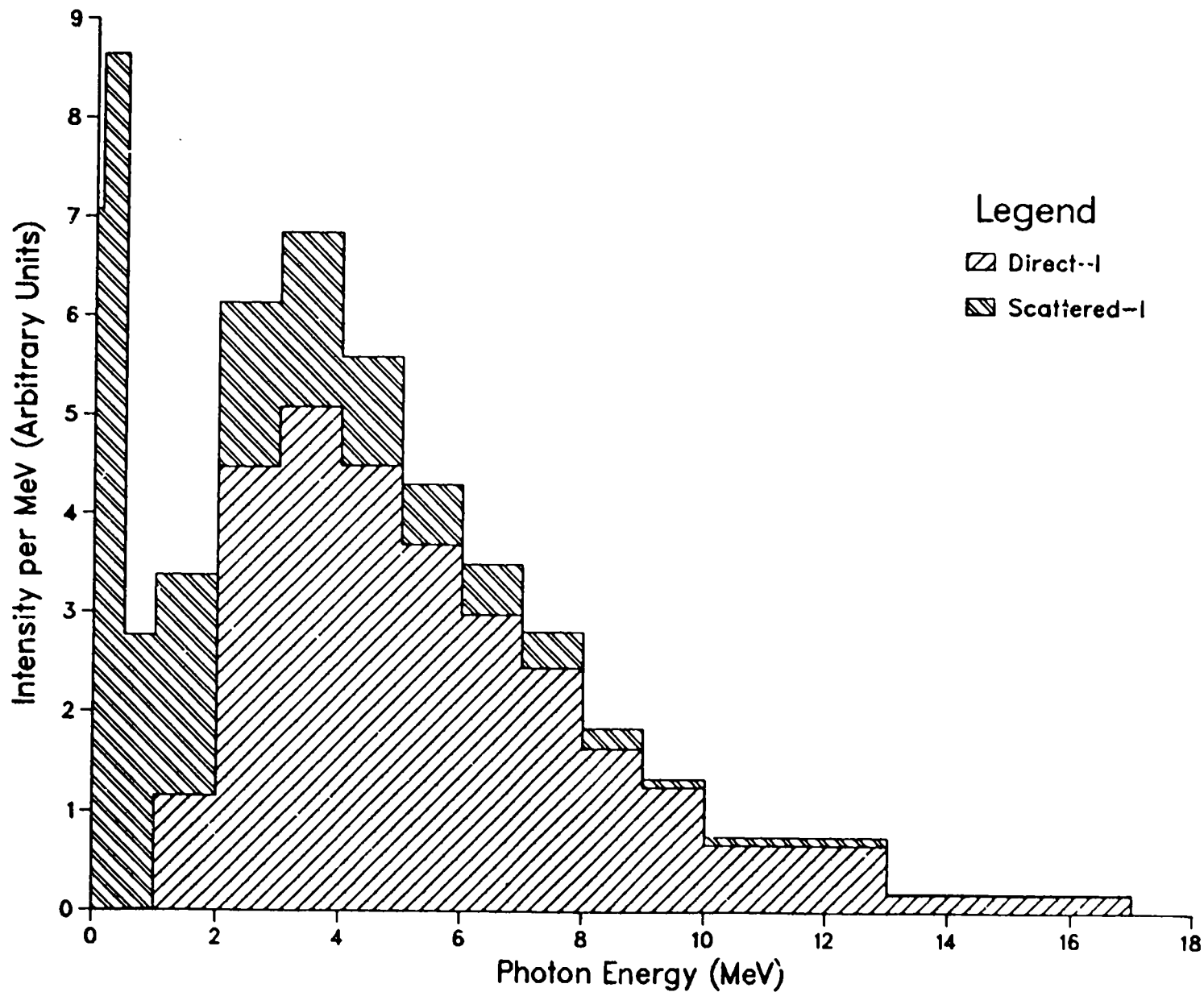
Fig. 7. Effective energy spectrum after the film response of Fig. 4 is folded into the spectrum of Fig. 6. The lower energies are enhanced, and the 0.1 to 0.5 MeV energy bin contributes significantly to the total dose.
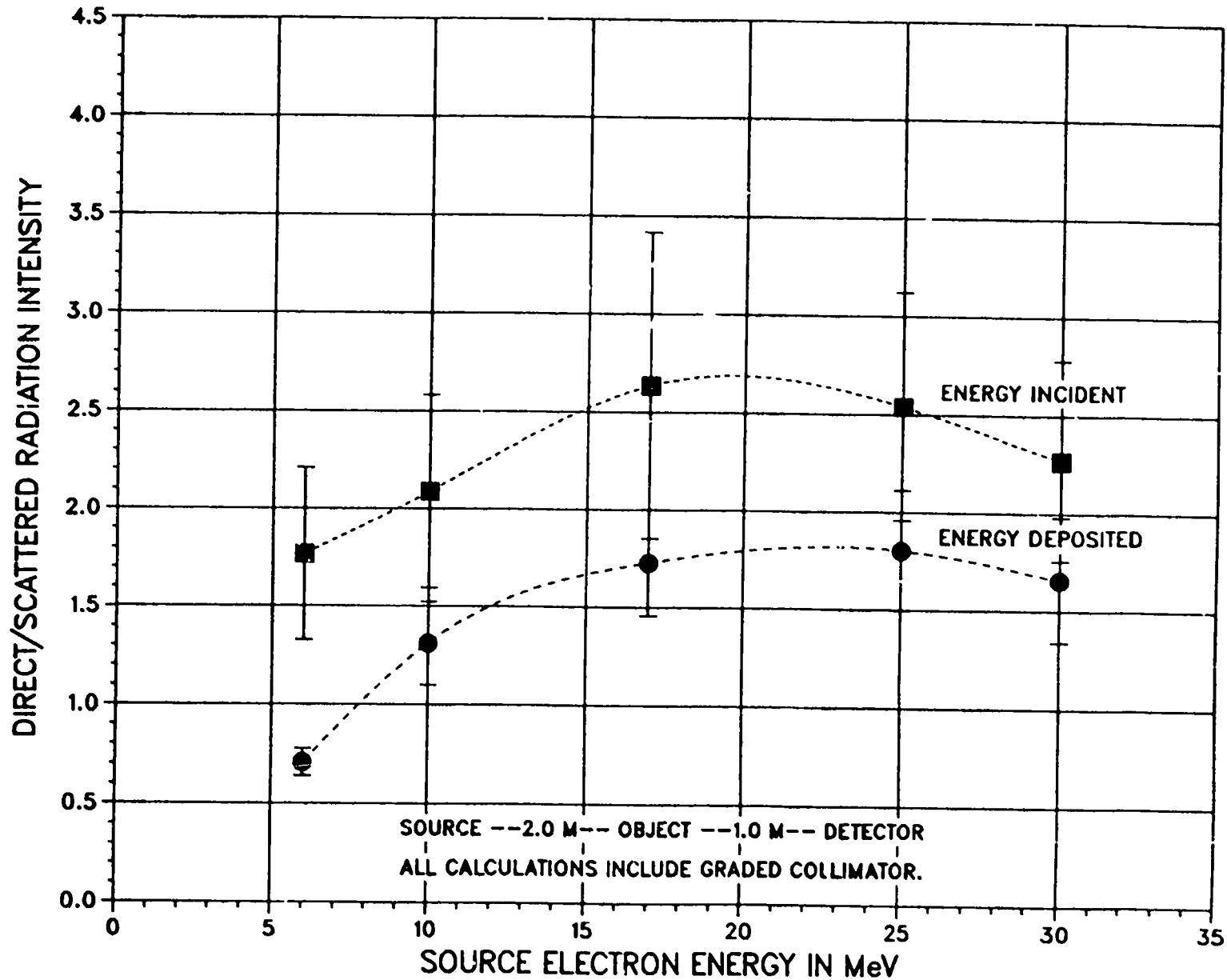
MCNP-E CALCULATIONS
MULTI-HOLE COLLIMATOR SIMULATIONS

Fig. 8. The multihole collimator was calculated in a way that simulates the treatment of the data from the NIH experiments. The results are plotted on the scale of Fig. 5, so that direct comparisons may be made.
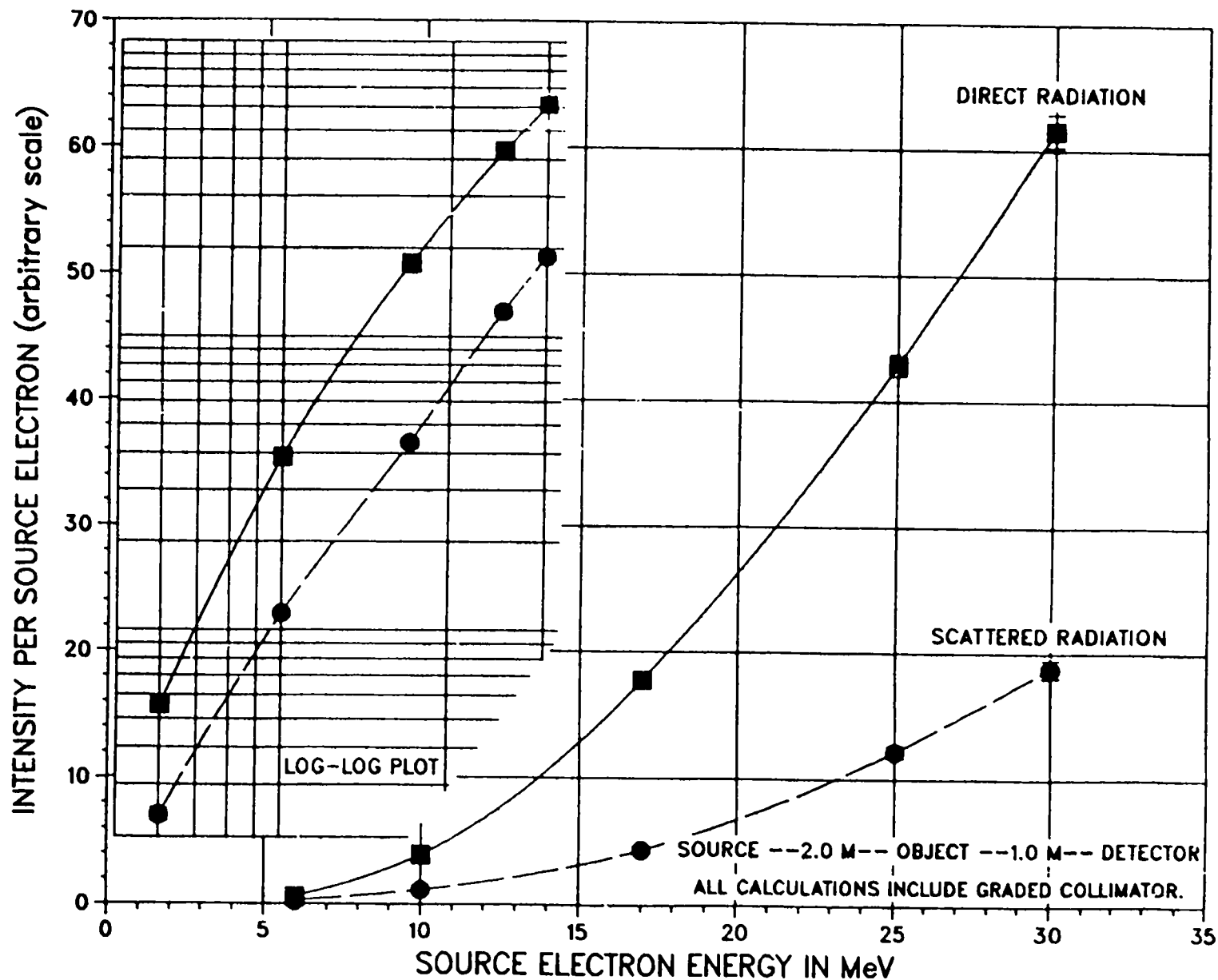
Fig. 9. Total dose at film plane, as a function of energy, for both direct and scattered radiation components. The source bremsstrahlung has, of course, been modified by the object.

MCNP-E CALCULATIONS
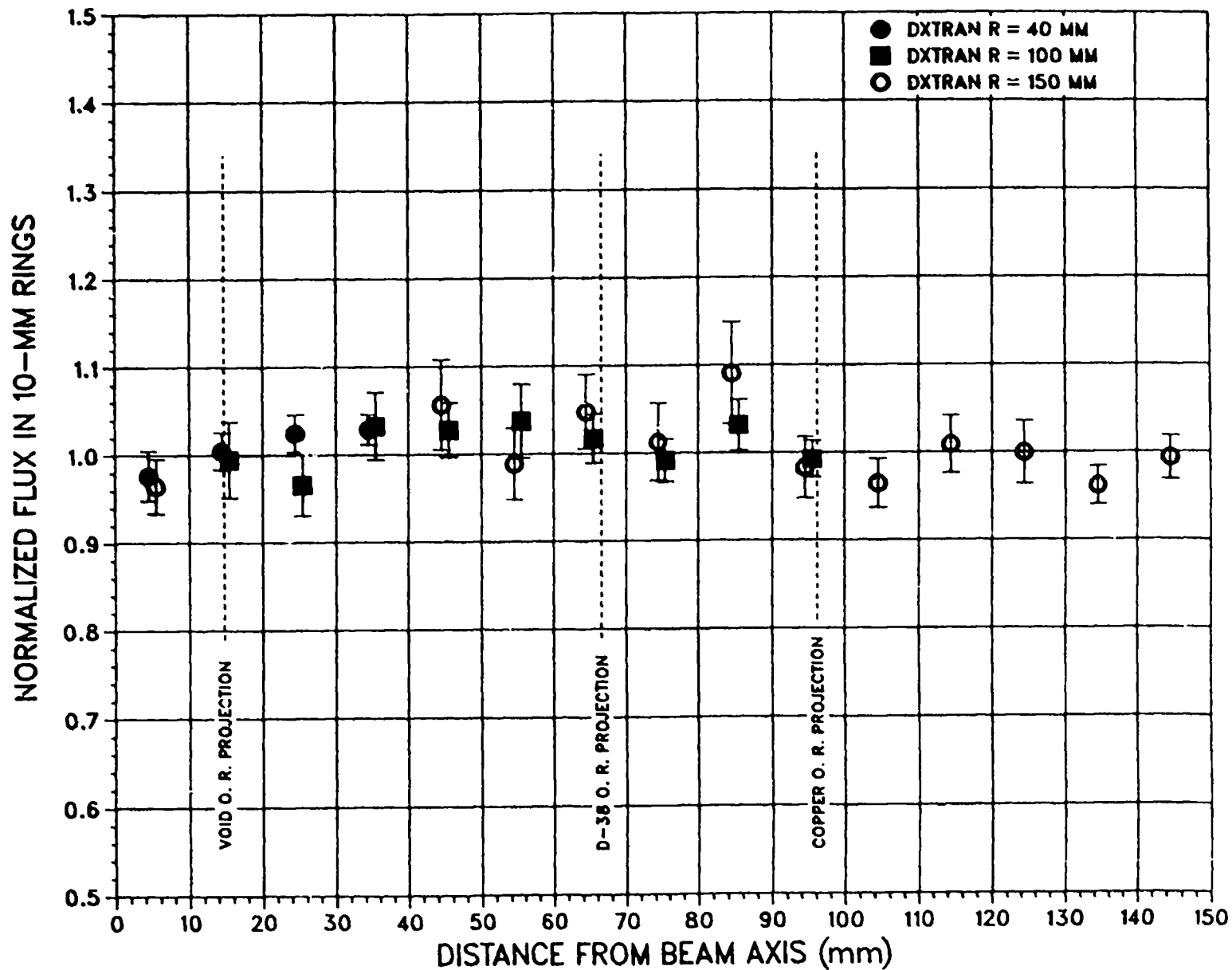## 17-MeV SCATTERED RADIATION PROFILE

Fig. 10. The scattered radiation in the film plane has been divided into 10-mm-wide rings concentric with the axis. A source of $3x10^6$ electrons has been used for all calculations except the open circle at the far left, which comes from the 17-MeV point in Fig. 5 (DXTRAN radius at 10 mm).